ACS APPLIED NANO MATERIALS

Article

www.acsanm.org

Seed-Layer Free Zinc Tin Oxide Tailored Nanostructures for Nanoelectronic Applications: Effect of Chemical Parameters

Ana Rovisco, Rita Branquinho, Jorge Martins, Maria João Oliveira, Daniela Nunes, Elvira Fortunato, Rodrigo Martins, and Pedro Barquinha*

i3N/CENIMAT, Department of Materials Science, Faculty of Science and Technology, Universidade NOVA de Lisboa and CEMOP/UNINOVA, Campus de Caparica, 2829-516 Caparica, Portugal

Supporting Information

ABSTRACT: Semiconductor nanowires are mostly processed by complex, expensive, and high temperature methods. In this work, with the intent of developing zinc tin oxide nanowires (ZTO NWs) by low-cost and low-complexity processes, we show a detailed study on the influence of chemical parameters in the hydrothermal synthesis of ZTO nanostructures at temperatures of only 200 °C. Two different zinc precursors, the ratio between zinc and tin precursors, and the concentration of the surfactant agent and of the mineralizer were studied. The type and the crystallinity of the nanostructures were found to be highly dependent on the used precursors and on the concentration of each reagent. Conditions for obtaining different ZTO nanostructures were achieved, namely, Zn_2SnO_4 nanoparticles and $ZnSnO_3$ nanowires with length ~600 nm, with the latter being reported for the first time ever by hydrothermal methods without the use of seed layers. Optical and electrical properties were analyzed, obtaining band gaps of 3.60 and 3.46 eV for $ZnSnO_3$ and Zn_2SnO_4, respectively, and a resistivity of 1.42 kΩ·cm for single $ZnSnO_3$ nanowires, measured using nanomanipulators after localized deposition of Pt electrodes by e-beam assisted gas decomposition. The low-temperature hydrothermal methods explored here proved to be a low-cost, reproducible, and highly flexible route to obtain multicomponent oxide nanostructures, particularly ZTO NWs. The diversity of the synthesized ZTO structures has potential application in next-generation nanoscale devices such as field effect nanotransistors, nanogenerators, resistive switching memories, gas sensors, and photocatalysis.

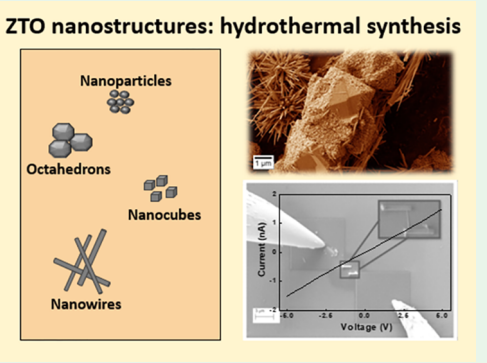

KEYWORDS: *nanostructure, nanowire, Zn_2SnO_4, $ZnSnO_3$, hydrothermal synthesis, ZTO*

INTRODUCTION

The increasing demand to have smart and multifunctional surfaces on all sorts of objects and shapes is pushing flexible and transparent electronics to unprecedented performance and integration levels.[1] For this end, it is highly desirable a material system offering sustainability in terms of raw materials and processes to synthesize its low-dimensional structures, combined with a wide range of properties to enable its use on transistors, sensing, or even energy-harvesting components. Metal oxides are one of the material classes with the highest potential to fulfill all these needs. In fact, ZnO-based nanostructures have been widely explored over the past decade.[2,3] ZnO nanowires are a good example of the multifunctionality of oxides, enabling for instance nano-generators to act as gas sensors and biosensors.[4,5] Moving from single to multicomponent oxides, e.g., from ZnO to zinc tin oxide (ZTO), has been one of the current trends, enabling one to obtain different properties by adjusting the cationic ratio, resulting in a wider range of applications for a given material system.[6] Concerning sustainability, ZTO also has a great advantage over other multicomponent oxides as the well-established indium−gallium−zinc oxide (IGZO) in thin-film technologies, since it avoids the use of critical raw materials as In and Ga.[7]

ZTO can crystallize through solid-state reaction in the metastable perovskite (orthorhombic or face centered, fcc)[8] or rhombohedral[9] forms ($ZnSnO_3$) and the more stable inverse spinel orthostannate (Zn_2SnO_4).[10,11] In Figure S1 in Supporting Information the crystalline structure of both phases is presented.

Zn_2SnO_4 is an n-type semiconductor with mobilities higher than 10−15 $cm^2\ V^{-1}\ s^{-1}$ and a wide band gap of 3.6 eV being reported in nanostructures.[12] On the other hand, $ZnSnO_3$ has been reported as an excellent piezoelectric material, with a piezoelectric potential along the *c*-axis of ~59 $\mu C/cm^2$, more than 1 order of magnitude higher than that of ZnO (~5 $\mu C/cm^2$),[13−15] and also as a ferroelectric material.[16] Its band gap was reported as being 3.9 eV, higher than for Zn_2SnO_4.[17,18] These ZTO nanostructures can be synthesized by vapor phase processes as chemical vapor deposition (CVD)[19] and thermal

Received: May 7, 2018
Accepted: July 20, 2018
Published: July 20, 2018

DOI: 10.1021/acsanm.8b00743
ACS Appl. Nano Mater. XXXX, XXX, XXX−XXX

evaporation,[6] which present high efficiency. However, these are cumbersome and expensive techniques, which demand high temperatures (>700 °C). Thereby, solution-based methods are imperative to decrease complexity, cost, and temperature while still enabling good performance of the synthesized nanostructures. Solution-based hydrothermal methods were already used to obtain ZTO nanostructures such as nanoparticles (NPs),[20] nanowires (NWs),[21] nanorods,[22] octahedrons,[23] nanocubes (NCs),[24,25] and nanoflowers.[26] These nanostructures have demonstrated interesting properties for numerous applications as photocatalysis,[27] sensors,[28−30] nanogenerators,[31−33] resistive switching memories,[34,35] and solar cells,[36] reinforcing the multifunctionality of ZTO for next-generation nanoscale devices.

A proper control of the synthesis process to achieve the target structure and shape is crucial. As an example, for gas sensing it was already reported that within $ZnSnO_3$ structures an orthorhombic phase (as the one obtained in this study) possesses a much higher sensibility than the fcc. The dimension of the obtained structures also plays an important role, with higher specific surface areas resulting in improved gas sensing performance.[37]

However, two important drawbacks need to be solved: first, it is well-known that obtaining a single phase ($ZnSnO_3$ or Zn_2SnO_4) and a single nanostructure shape (e.g., NP or NW) by solution processes is quite challenging.[38,39] This can limit the usefulness of ZTO for different applications, as the properties are heavily dependent on phase and shape; also, low-cost hydrothermal methods, highly desirable from an upscaling perspective, always require seed layers to achieve $ZnSnO_3$ NWs.[38,40] While the use of a seed layer can enable easier fabrication of vertical structures such as gate-all-around transistors,[41,42] synthesizing ZTO NWs without a seed layer also brings multiple advantages: imposes fewer constraints to the synthesis conditions to be studied, which is crucial for investigating in detail the role of each synthesis parameter in controlling phase, shape, and size of the nanostructures;[10,43] allows for fewer processing steps to obtain the nanostructures; provides higher degree of freedom to integration by relying on a wide variety of available transfer methods to obtain random and aligned networks of NWs on any substrate;[44] finally, the nanostructures do not incorporate on their final shape any undesired residuals from the seed layers.[45]

In this paper, we present different multicomponent ZTO nanostructures produced by a seed-layer-free, one-step hydrothermal method, at only 200 °C. The chemical and structural influence on the solution-based synthesis of the zinc salt, the ratio between zinc and tin precursors, the concentration of the surfactant agent (H_2O:EDA ratio), and the mineralizer (NaOH) concentration were studied with the aim of obtaining ZTO NWs. We are particularly interested in 1D structures given their efficient charge transport, crucial for conceiving nanoelectronic devices.[46]

Herein we show a simple hydrothermal method where we can control the phase and shape of the nanostructures by tuning the chemical parameters of the synthesis. $ZnSnO_3$ NWs were successfully achieved without the support of seed layers and using two different zinc precursors.

RESULTS AND DISCUSSION

Introduction: Governing Equations To Obtain ZTO NWs. In a typical hydrothermal method to achieve ZTO nanostructures, the synthesis product is seldom composed by a single crystalline phase. In fact, $ZnSnO_3$ NWs, Zn_2SnO_4 NPs, NCs and octahedrons with nanoplates, ZnO NWs, SnO_2 NPs and mixtures of them are usually obtained (Figure S2).[10] It is thus imperative to revise the governing equations representing the chemical processes to achieve each of these phases when Zn and Sn precursors are present.

The chemical reaction processes for the formation of $ZnSnO_3$ nanostructures can be represented by the following equations:[47]

$$Zn^{2+} + Sn^{4+} + 6OH^- \rightarrow ZnSn(OH)_6$$

$$ZnSn(OH)_6 \rightarrow ZnSnO_3 + 3H_2O$$

Concerning Zn_2SnO_4, its formation can be represented as follows:[12,43]

$$Zn^{2+} + Sn^{4+} + 6OH^- \rightarrow ZnSn(OH)_6\downarrow$$

$$Zn^{2+} + 4OH^- \rightarrow Zn(OH)_4^{2-}$$

$$ZnSn(OH)_6 + Zn(OH)_4^{2-} \rightarrow Zn_2SnO_4 \downarrow + 4H_2O + 2OH^-$$

While these equations provide an ideal scenario to obtain $ZnSnO_3$ and Zn_2SnO_4 nanostructures, it has to be taken into account that the modification of the concentration of the precursors and the mineralizer during the reaction can promote the formation of other species/structures. Moreover, both ZTO phases have $ZnSn(OH)_6$ as an intermediary phase (Figure S2), which can also appear as an end product for synthesis with short durations and/or low temperatures. Given this, the detection of OH^- groups by FTIR spectroscopy is quite useful for inferring about the completeness of the reaction (Figure S3).

Regarding the formation of ZnO nanostructures, it is normally associated with a high alkaline concentration,[43] and it can be represented by

$$Zn(OH)_4^{2-} \rightarrow ZnO \downarrow + H_2O + 2OH^-$$

where tin species are washed away after reaction.

Finally, with respect to the SnO_2 nanostructures,[43] its formation is favored by a lower alkaline concentration and can be represented by the following equation:

$$Sn^{4+} + 3H_2O \leftrightarrow H_2SnO_3 + 4H^+$$

$$H_2SnO_3 \rightarrow SnO_2 \downarrow + H_2O$$

$$H^+ + OH^- \rightarrow H_2O$$

Similar to tin species in the case of a highly alkaline environment, the zinc species are washed away after synthesis.

While the cationic ratios and chemical parameters mentioned above dictate which nanostructures within the Zn−Sn−O system are obtained, understanding the growth mechanism for each nanostructure would require a detailed analysis of the effect of physical parameters such as time, temperature, and pressure,[43,48,49] which is currently underway.

Influence of the Zn:Sn Molar Ratio. The type of precursor and the ratio between the metallic elements in the synthesis are crucial to define the nanostructures' shape, size, and crystallinity. We first studied the different ratios between zinc and tin precursors (2:1, 1:1, and 1:2) using two different zinc sources, zinc acetate (ZnAc) and zinc chloride ($ZnCl_2$).

DOI: 10.1021/acsanm.8b00743
ACS Appl. Nano Mater. XXXX, XXX, XXX−XXX

For these studies a NaOH molar concentration of 0.240 M and a H_2O:EDA volume ratio of 7.5:7.5 mL:mL were used, based on the synthesis reported by Li et al.,[12] where Zn_2SnO_4 NWs were grown on a stainless steel mesh for dye-sensitized solar cells application.

Synthesis using ZnAc as the Zn precursor, with a Zn:Sn molar ratio of 1:2, results in inconclusive XRD analysis, showing the possible presence of different phases whose diffraction peaks overlap (Figure 1a): tetragonal phase of SnO_2

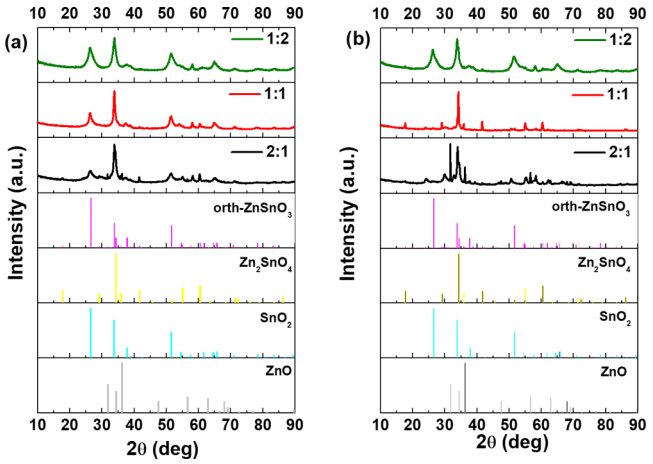

Figure 1. XRD patterns for three different Zn:Sn molar ratios (1:2, 1:1, and 2:1) using (a) ZnAc precursor and (b) $ZnCl_2$ precursor. Identification is following ICDD cards 00-028-1486 (deleted), 00-024-1470, and 01-077-0452 (Figure S2).

(ICDD card 01-077-0452), $ZnSnO_3$ orthorhombic perovskite phase, and Zn_2SnO_4 inverse spinel phase (ICDD card 00-024-1470). For the $ZnSnO_3$ orthorhombic perovskite phase, peaks can be identified by the ICDD card 00-028-1486. It should be noted that although this card was removed from the ICDD database due to the similarities with a mixture of Zn_2SnO_4 and SnO_2 phases, several reports in the literature[48,50−52] still refer to it. In fact, when we performed peak indexing in different $ZnSnO_3$ nanowires samples, an orthorhombic phase was always determined. These findings are also supported by Raman analysis as will be discussed later.

SEM analysis (Figure 2a) supports the argument that some ZTO ($ZnSnO_3$ and/or Zn_2SnO_4) NWs are starting to form. This is reinforced by Raman spectroscopy analysis (Figure S4a), which shows the predominance of the vibrational band at 631 cm^{-1} associated with the expansion and contraction of the Sn−O bond peak[53] but also that peaks at 538 and 676 cm^{-1} start to appear, corresponding to internal vibrations of the oxygen tetrahedron in Zn_2SnO_4 and to the characteristic Raman M−O bonds stretching vibration mode in the MO_6 octahedron of $ZnSnO_3$ and/or Zn_2SnO_4, respectively.[43]

For synthesis with a 1:1 molar ratio of Zn:Sn, $ZnSnO_3$ NWs are predominantly obtained, as shown by XRD and SEM analysis (Figure 1b and Figure 2b). The identification of ortho-$ZnSnO_3$ is not immediately clear: it can be mistaken not only with SnO_2 (as seen before for 1:2 Zn:Sn molar ratio) but also with Zn_2SnO_4 inverse spinel-cubic phase (ICDD card 00-024-1470). EDS analysis on isolated wires shows the ratio Zn:Sn of 1:1 (Figure S5), supporting the $ZnSnO_3$ phase, which was also identified by Kovacheva et al.[54] on a similar XRD spectra. Raman spectroscopy shows that the intensity of the 676 cm^{-1} peak (Zn_2SnO_4 or $ZnSnO_3$) increases while the intensity for

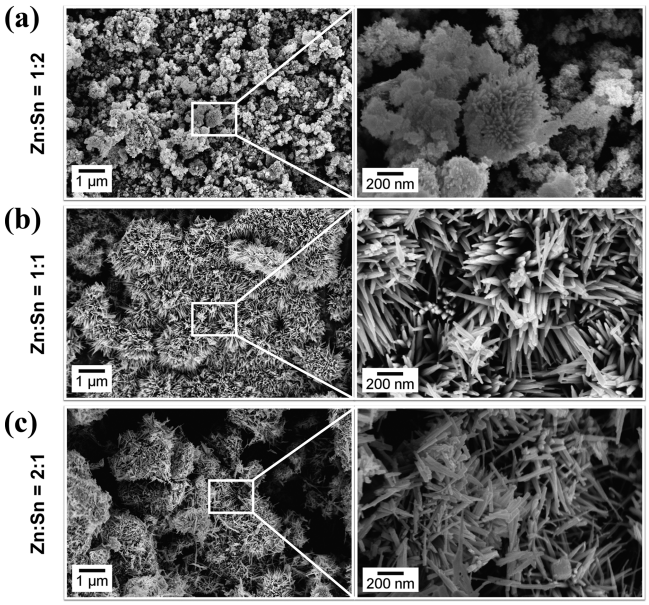

Figure 2. SEM micrographs of nanostructures obtained with ZnAc precursor and Zn:Sn molar ratios of (a) 1:2, (b) 1:1, and (c) 2:1.

the 538 cm^{-1} peak (Zn_2SnO_4) decreases when compared with the sample using 1:2 Zn:Sn ratio. This confirms the predominance of the $ZnSnO_3$ phase for the ratio 1:1. (Figure S4a). While SnO_2 NPs could not be confirmed by SEM analysis, deeper investigation using SEM and EDS revealed a plausible explanation for the SnO_2 peak: Figure S5 shows that within the same sample some structures comprising agglomerated NWs could be found. Such structures were reported by Mao et al.[55] and have been described as ZnO-doped SnO_2. This can be explained by the higher solubility of chlorides in solvents based on ethylenediamine when compared to acetates: the prior dissolution of tin chloride would lead initially to the formation of SnO_2 nanostructures, which could then be doped by the Zn present in the solution, which falls in line with the Zn and Sn distribution measured by EDS as seen in Figure S6 (see also Figure S7).

XRD data obtained for the synthesis with Zn:Sn molar ratio of 2:1 are similar to the data of 1:1 condition (Figure 1b), suggesting the presence of $ZnSnO_3$ perovskite phase. However, SEM in Figure 2c readily shows that besides the $ZnSnO_3$ NWs some other structures are present. A more detailed analysis reveals a mixture of $ZnSnO_3$ and Zn_2SnO_4 octahedrons and NWs, microtubes comprising agglomerates of $ZnSnO_3$ NWs and ZnO nanoplatelets (Figure S8 and Figure S9). Raman spectroscopy data support these results, showing the predominance of the 676 cm^{-1} peak associated with $ZnSnO_3$ and/or Zn_2SnO_4 over the 631 cm^{-1} peak from SnO_2 but also the presence of the 538 cm^{-1} peak corresponding to Zn_2SnO_4. Furthermore, a small peak at 574 cm^{-1} is detected for this synthesis condition, attributed to a vibrational mode of ZnO,[56] concomitant with the SEM analysis.

It can be concluded that for the ZnAc precursor a 1:1 Zn:Sn molar ratio is the one allowing us to obtain $ZnSnO_3$ NWs without a large fraction of other Zn- and/or Sn-based nanostructures. As such, this ratio was chosen for the following studies. It should be noted that Li et al. reported Zn_2SnO_4 NWs following a similar synthesis but using a stainless steel mesh as seed, favoring the growth of ZTO nanostructures similar to the cubic structure of the seed.[12]

DOI: 10.1021/acsanm.8b00743
ACS Appl. Nano Mater. XXXX, XXX, XXX−XXX

The same study was performed using $ZnCl_2$ as zinc precursor, with the different Zn:Sn molar ratios of 1:1, 1:2, 2:1. Using a Zn:Sn molar ratio of 1:2, similar XRD data are obtained when compared to the ZnAc precursor, suggesting that a tetragonal phase of SnO_2 and/or a $ZnSnO_3$ perovskite phase exists (Figure 1b). SEM analysis reveals that both SnO_2 NPs and ZTO ($ZnSnO_3$ and/or Zn_2SnO_4) NWs are obtained but now with more relevance to the latter (Figure 3a). Raman spectroscopy data confirm this, exhibiting a more intense peak for $ZnSnO_3$ and/or Zn_2SnO_4 (676 cm^{-1}) than for SnO_2 (636 cm^{-1}), as seen in Figure S4b.

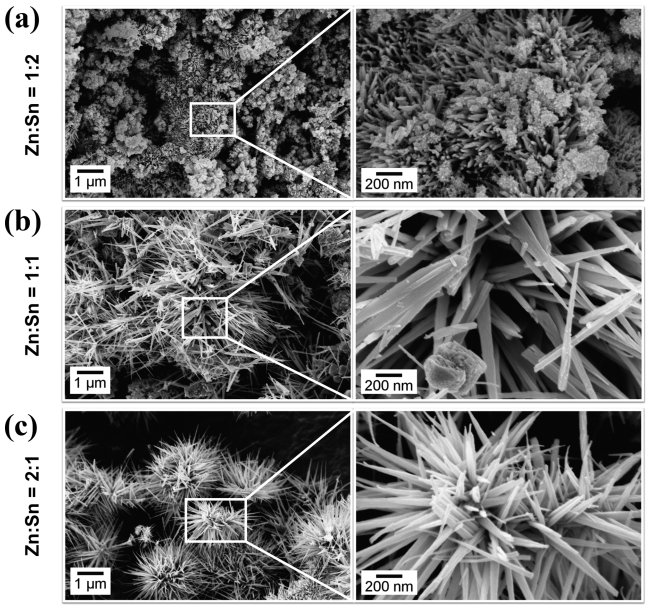

Figure 3. SEM micrographs of nanostructures obtained with $ZnCl_2$ precursor and Zn:Sn molar ratios of (a) 1:2, (b) 1:1, and (c) 2:1.

For a solution with Zn:Sn molar ratio of 1:1, the XRD spectra show mainly the phase Zn_2SnO_4, as depicted in Figure 1b, with some small peaks attributed to $ZnSnO_3$ and SnO_2. SEM images show several types of nanostructures: while $ZnSnO_3$ NWs are clearly observed (Figure 3b), a more detailed inspection also reveals a large amount of Zn_2SnO_4 NCs (Figure S10). For the Zn:Sn molar ratio of 2:1 mostly $ZnSnO_3$ NWs are obtained (Figure 3c). Still, a few ZnO columnar nanoplatelets with hexagonal phase (ICDD card 00-036-1451) are also shown in Figure S11c. These trends are confirmed by the Raman analysis (Figure S4b), analyzing the evolution of peaks at 538 cm^{-1} (Zn_2SnO_4), 676 cm^{-1} (Zn_2SnO_4 and/or $ZnSnO_3$), and 631 cm^{-1} (SnO_2). Similar structures were already reported by Tian et al.[57] for the synthesis of ZnO nanostructures. Figure S11a shows an example of $ZnSnO_3$ NW agglomerates obtained in this condition, which is shown by EDS to have a 1:1 Zn:Sn ratio (Figure S12). Curiously, by looking at the hexagonal form in the middle, we can suggest that the ZTO NWs are grown from an initial hexagonal ZnO microtube/wire. The initial formation of the ZnO NWs can be attributed to the higher solubility of $ZnCl_2$ when compared to $SnCl_4{\cdot}5H_2O$,[55] contributing to the faster formation of these structures relative to the $ZnSnO_3$ NWs, which is an issue when trying to obtain single phase ZTO nanostructures. However, according to Miyauchi et al., these ZnO NWs can be removed with an acid solution of HNO_3,[17] allowing us to achieve only $ZnSnO_3$ NWs in the sample. As such, the Zn:Sn ratio of 2:1 was the selected condition for the following studies with the $ZnCl_2$ precursor, allowing us to obtain $ZnSnO_3$ NWs with an average length of 605 nm and a diameter of around 65 nm.

For both zinc precursors, for the Zn:Sn molar ratio of 1:2, SnO_2 NPs are predominantly obtained, which can be attributed to the higher concentration of tin precursor in the solution. Even so, the initial growth of $ZnSnO_3$ NWs is already observed. When the molar ratio is 1:1, the results differ for the two precursors. For ZnAc this was shown to be the best ratio in terms of promoting the growth of a single phase of $ZnSnO_3$ NWs. On the other hand, for $ZnCl_2$, this ratio leads to a mixture of Zn_2SnO_4 NCs (predominant) and $ZnSnO_3$ NWs. As for the 2:1 molar ratio of Zn:Sn, it is the condition that promotes better results when using $ZnCl_2$, resulting in $ZnSnO_3$

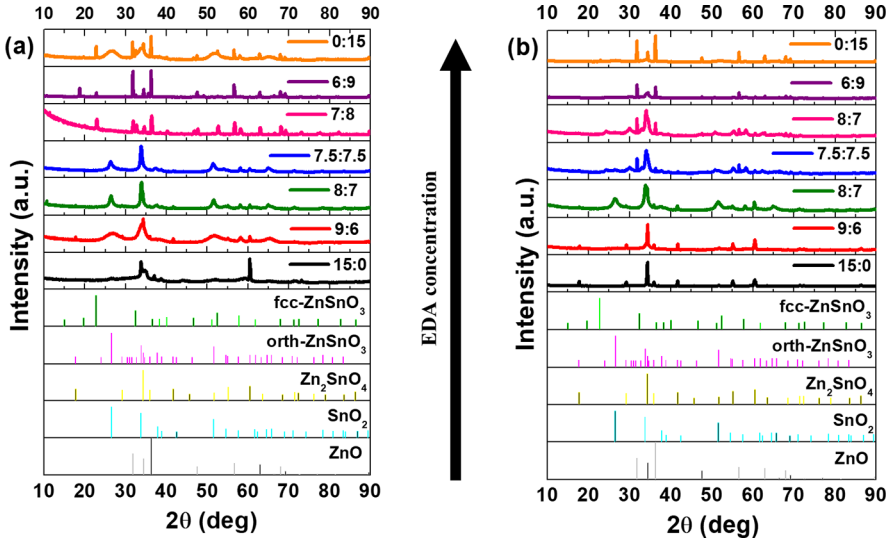

Figure 4. XRD patterns when using (a) ZnAc precursor (with 1:1 Zn:Sn ratio) and (b) $ZnCl_2$ precursor (with 2:1 Zn:Sn ratio) for different H_2O:EDA volume ratios. Identification is following ICDD cards 00-028-1486 (deleted), 00-011-0274, 00-024-1470, 01-077-0452, and 00-06-1451 (Figure S2).

DOI: 10.1021/acsanm.8b00743
ACS Appl. Nano Mater. XXXX, XXX, XXX−XXX

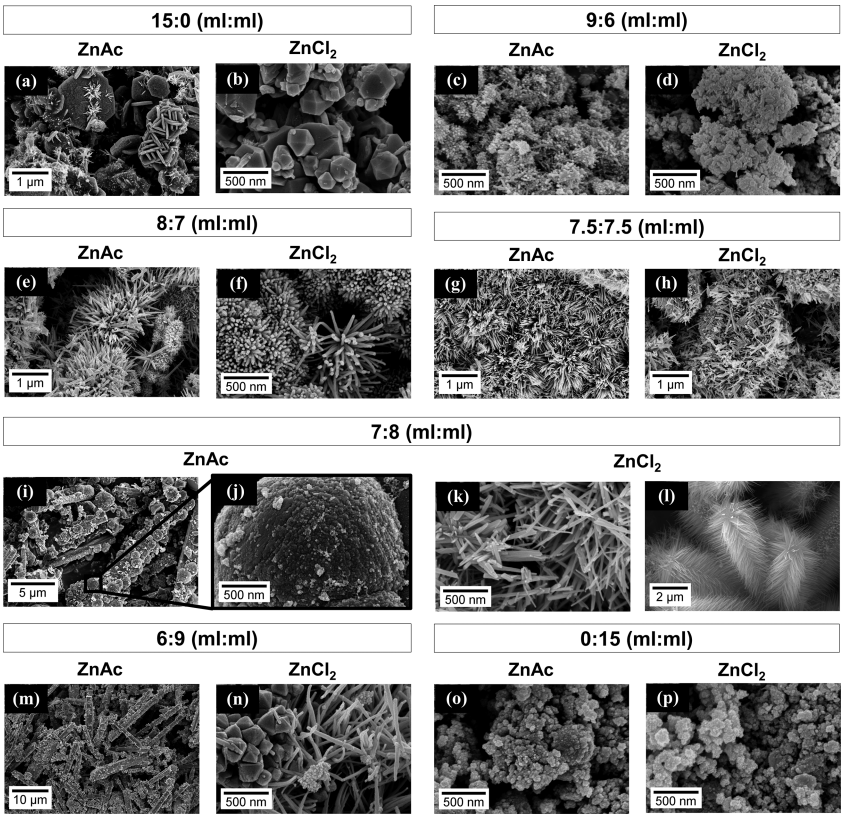

Figure 5. SEM micrographs of the nanostructures obtained by synthesis using ZnAc/$ZnCl_2$ as precursors, respectively, with the different H_2O:EDA volume ratios of (a, b) 15:0, (c, d) 9:6, (e, f) 8:7, (g, h) 7.5:7.5, (i–l) 7:8, (m, n) 6:9, and (o, p) 0:15.

NWs (although mixed with ZnO NWs), while for ZnAc a higher mixture of phases, with predominance of Zn_2SnO_4 NCs, is achieved.

In summary, whichever the ratios, using ZnAc promotes the presence of SnO_2 while using $ZnCl_2$ results in higher amounts of ZnO. This can be explained by the different precursors' solubility: while $SnCl_4{\cdot}5H_2O$ is more soluble than ZnAc, promoting a faster growth of tin-based structures, $ZnCl_2$ is more soluble than tin chloride, promoting a preferential growth of zinc-based structures. Table S1 presents the nanostructures sizes for the different conditions of both zinc precursors, obtained through the SEM images and using the software ImageJ. In general, it is possible to observe that the nanostructures produced using $ZnCl_2$ as zinc precursor have longer sizes than the nanostructures produced using ZnAc.

Influence of the Surfactant Concentration. Oriented growth and morphological control of nanostructures are highly dependent on surfactant use.[43] This section presents the study of the influence of the H_2O:EDA volume ratio for the two selected conditions from the previous study: Zn:Sn = 1:1 molar ratio using the ZnAc precursor and Zn:Sn = 2:1 molar ratio using the $ZnCl_2$ precursor. The H_2O:EDA volume ratios used were 15:0, 9:6, 8:7, 7.5:7.5, 8:7, 9:6, and 15:0 mL:mL. For all conditions the mineralizer's (NaOH) concentration was kept as 0.240 M.

For the ZnAc precursor and using only H_2O as a solvent a mixture of $ZnSnO_3$ NWs and Zn_2SnO_4 nanoplates and octahedrons comprising nanoplates is obtained (Figure 4a and Figure 5a), with Zn_2SnO_4 being the predominant phase. These types of octahedron structures were already reported by Ji et al.[23] With increasing of EDA up to 7.5:7.5, there is a trend for Zn_2SnO_4 NPs to disappear while $ZnSnO_3$ NWs dimensions get larger. SnO_2 NPs initially appear as isolated structures moving to SnO_2-filled $ZnSnO_3$ NWs as EDA volume is increased (Figure 4a, Figure 5, and Figure S13a). For 7:8 volume ratio, there is an increase in the presence of ZnO NWs and $ZnSnO_3$ NPs with face centered cubic structure (Figure 4a and Figure 5i,j), due to the higher amount of EDA. Note that $ZnSnO_3$ face centered cubic structure and $ZnSn(OH)_6$ exhibit coincident Raman peak (603 cm^{-1})[49] and XRD peaks (Figures S13 and S2, respectively). Still, for this synthesis condition it is verified by FTIR analysis that no OH^- groups are present (Figure S14), confirming the $ZnSnO_3$ identification. The ratio 6:9 produces mainly ZnO NWs and only a few $ZnSnO_3$ NPs as shown by SEM and XRD (Figure 5m and Figure 4a, respectively). When no H_2O is used as solvent (0:15), mostly SnO_2 NPs and ZnO NWs are obtained, with some $ZnSnO_3$ NPs being also present (Figure 4a and Figure 5o). These results are confirmed by Raman spectroscopy (Figure S13a) and can be explained by the significantly higher solubility of $SnCl_4{\cdot}5H_2O$ in EDA compared to ZnAc, inducing a faster and preferential growth of SnO_2 NPs and the later growth of ZnO NWs. Still, probably due to the long duration of the synthesis, some $ZnSnO_3$ NPs are grown, since as previously discussed ZTO nanostructures can originate from SnO_2 nanostructures.

For $ZnCl_2$ as precursor and when using only water as a solvent (15:0 H_2O:EDA), Zn_2SnO_4 NPs with octahedral shape are obtained (Figure 5b). The XRD spectra (Figure 4b) show a pure cubic-spinel-type phase for these nanostructures. This is the most stable phase and shape for zinc tin oxide in the absence of EDA, in line with the literature even for other conditions of hydrothermal synthesis.[23,58,59] With the addition

DOI: 10.1021/acsanm.8b00743
ACS Appl. Nano Mater. XXXX, XXX, XXX–XXX

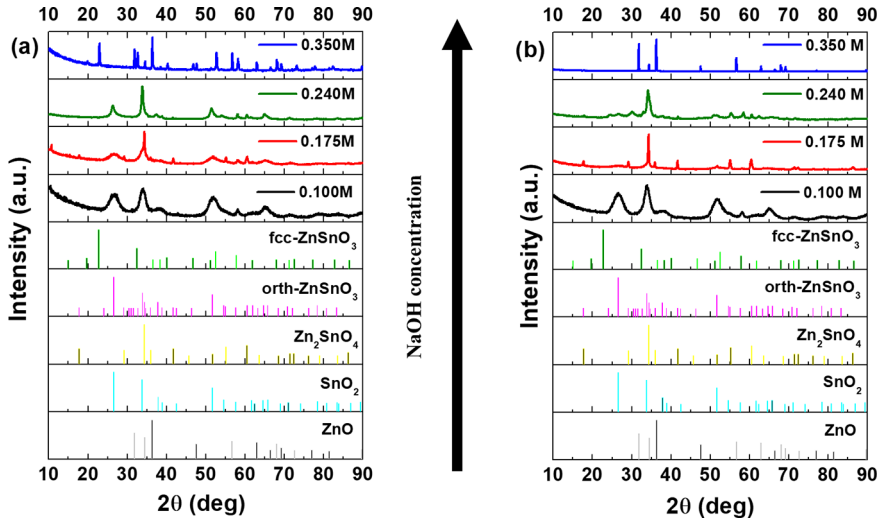

Figure 6. XRD pattern of the nanostructures obtained for different NaOH concentrations, using (a) ZnAc and (b) $ZnCl_2$ as zinc precursors. Identification is following ICDD cards 00-028-1486 (deleted), 00-011-0274, 00-024-1470, 01-077-0452, and 00-036-1451 (Figure S2).

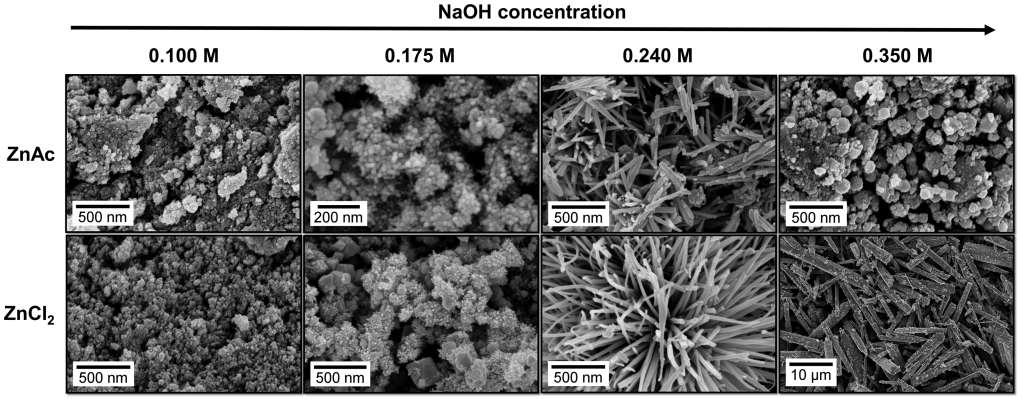

Figure 7. SEM micrographs of the nanostructures obtained by synthesis using different NaOH concentrations.

of EDA, for a H_2O:EDA ratio 9:6, Zn_2SnO_4 nanostructures with a different shape than the octahedral and some $ZnSnO_3$ NWs are obtained, as seen by SEM (Figure 5d). By XRD (Figure 4b), it can be verified the mixture of $ZnSnO_3$ and Zn_2SnO_4 phases, with Zn_2SnO_4 still being predominant. By increase of EDA's concentrations (8:7, 7.5:7.5, and 7:8), the size of $ZnSnO_3$ NWs is increased and this phase becomes predominant. As Figure 5f shows, for the 8:7 ratio, only $ZnSnO_3$ NWs are grown, but they present a large size distribution. For the 7.5:7.5 ratio, $ZnSnO_3$ and large wires of ZnO are obtained, as it was already discussed in section Introduction: Governing Equations To Obtain ZTO NWs. For the 7:8 ratio the $ZnSnO_3$ NWs are highly agglomerated, as shown in Figure 5l. These structures are similar to the obtained for ZnAc (7.5:7.5, Zn:Sn = 1:1), as described by Mao et al.[55] The H_2O:EDA ratio of 6:9 gives miscellaneous results, as Figure 5n and Figure S15 show, with a mixture of several types of structures being obtained. It is possible to observe Zn_2SnO_4 NCs and octahedrons comprising nanoplates, $ZnSnO_3$ NWs, SnO_2 NPs, and also ZnO columnar nanoplatelets agglomerates, with all of these phases being identified by XRD (Figure 4b). By use of only EDA (0:15), $ZnSnO_3$ NPs and ZnO NWs are formed (Figure 5p). The strong ZnO peaks in XRD (Figure 4b) appear due to the large size of ZnO NWs when comparing with the $ZnSnO_3$ NPs. Overall, the XRD (Figure 4b) shows that for higher EDA's concentration, the formation of ZnO becomes preferential over ZTO, which is in agreement with the SEM/EDS and Raman (Figure S13b) analysis. This preferential formation of ZnO nanostructures for the higher EDA conditions can be explained by the strong coordination ability between the $ZnCl_2$ and EDA molecules.[60,61]

FTIR analysis helps us to understand and to explain the results for the synthesis where EDA has a higher concentration than H_2O. Figure S14a shows that when using ZnAc as zinc precursor, for the conditions with H_2O:EDA ratios of 7:8, 6:9, and 0:15, precursor or solvent residuals are still present in the final product, due to the low solubility of ZnAc in EDA. In comparison, for the synthesis using $ZnCl_2$, residuals are observed when only EDA is used as a solvent (Figure S14.b), which can be attributed to the higher solubility of $ZnCl_2$ in EDA, compared to that of ZnAc. For all the other conditions no precursor peaks can be traced by FTIR analysis.

Table S2 summarizes the type of nanostructures obtained for the different conditions and their respective dimensions. The trend verified in the previous study regarding the longer sizes of nanostructures synthesized using $ZnCl_2$ as compared to ZnAc is again observed here. It is also reinforced the higher presence of Sn-based structures in the synthesis using ZnAc, and a predominance of Zn-based structures in the synthesis using $ZnCl_2$. The addition of EDA favors the formation of $ZnSnO_3$ NWs over the more energetically stable Zn_2SnO_4 NPs, which we attribute to the pH increase, as reported by

DOI: 10.1021/acsanm.8b00743
ACS Appl. Nano Mater. XXXX, XXX, XXX−XXX

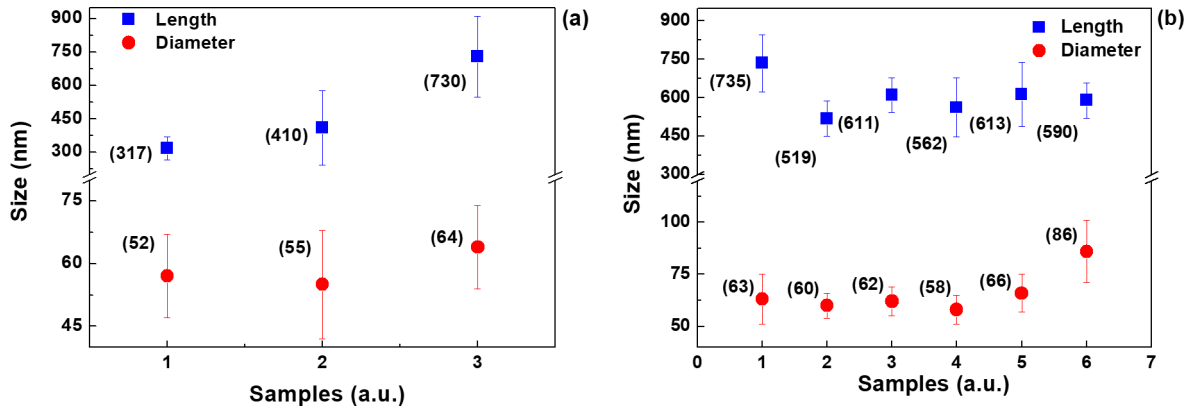

Figure 8. Comparison of the obtained nanostructures dimensions in different repetitions of synthesis using (a) ZnAc and (b) $ZnCl_2$ as zinc precursor, under similar conditions. Average lengths and diameters are given in parentheses.

Miyauchi et al.[17] Up to a certain EDA concentration the length and diameter of these NWs are increased. For both precursors, an optimal H_2O:EDA volume ratio of 7.5:7.5 was determined for the formation of $ZnSnO_3$ NWs. As the EDA concentration is increased beyond this point, ZnO nanostructures start to be dominant, even for the ZnAc precursor. This suggests that the predominant factor defining the type of nanostructure obtained in an environment with a high EDA concentration starts to be the pH value, as will be discussed in more detail in the next section. Thus, despite the relevance of EDA to achieve the desired ZTO NWs, the presence of the water is imperative to the formation of these nanostructures, not only to ensure the complete dissolution of the precursors but also to balance the pH in solution.

Influence of NaOH Concentration. NaOH plays an important role in the growth of the nanostructures, acting as a mineralizer agent, having a direct influence on the definition of the crystalline phase that is produced.

On the basis of the previous studies presented in this manuscript, the synthesis conditions for this study were set as Zn:Sn = 1:1 ratio when using the ZnAc precursor, Zn:Sn = 2:1 ratio with the $ZnCl_2$ precursor, keeping a H_2O:EDA ratio of 7.5:7.5 in both conditions. Concentrations of NaOH of 0.100 M, 0.175 M, 0.240 M, and 0.350 M were used to understand the influence of the mineralizer on the synthesis. The results for both zinc precursors presented the same trend, being discussed here simultaneously. The poorer concentration of NaOH (0.100 M) synthesis results in SnO_2 NPs, whichever precursor is used, as seen in Figures 6 and 7. Lehnen et al.[22] explained this behavior as an effect of the fast hydrolysis of Sn^{4+} cations, leading to the preferential formation of SnO_2. With the increasing of the NaOH concentration to 0.175 M, SnO_2 NPs are still obtained but Zn_2SnO_4 NPs are now predominant. Still, SnO_2 is more evident for the ZnAc precursor, as shown in the XRD spectra (Figure 6a), which would be expected based on the higher solubility of $SnCl_4 \cdot 5H_2O$ compared to ZnAc. Increasing the NaOH concentration to 0.240 M, the Zn_2SnO_4 phase is no longer present and $ZnSnO_3$ NWs are now produced, both in dispersed and in agglomerate shapes, as well as some ZnO NWs as already discussed in the section Influence of the Zn:Sn Molar Ratio. Finally, for the NaOH concentration of 0.350 M, only ZnO NWs are obtained when using $ZnCl_2$, while when using ZnAc both ZnO NWs and $ZnSnO_3$ NPs (ICDD card 00-011-0274) are observed. This trend of preferential growth of ZnO in alkaline solutions is well-known, since divalent metal ions do not hydrolyze in acidic environments.[62] Even with higher concentrations of NaOH (0.500 M) the resulting structures were verified to be the same as for 0.350 M but with a lower reaction yield. These results are in agreement with the literature, as Lehnen et al.[22] showed the same tendency for specific pH values: for pH ≈ 1 SnO_2 NPs are obtained, pH ≈ 8.5 yields Zn_2SnO_4 NPs, and higher pH values yields ZnO mixed with $ZnSn(OH)_6$.

Our results show a similar trend; i.e., lower pH leads to SnO_2 structures and higher pH favors ZnO ones, even if the starting pH (without adding NaOH) is already 12. As such, this trend is not dependent on the pH value itself but in the variation of the NaOH concentration for a specific synthesis.

Table S3 summarizes all these findings, showing that low mineralizer concentrations favor the growth of tin oxide structures over zinc oxide ones, with the trend being reversed as the NaOH concentration increases. Having in mind the specific goal of obtaining ZTO NWs, the optimum mineralizer concentration is around 0.240 M.

As seen in the previous sections, data in Figure 7 and Table S3 reinforce the trend of obtaining nanostructures with larger dimensions using $ZnCl_2$ precursor instead of ZnAc, given the higher solubility of $ZnCl_2$.

Reproducibility. For a comparison of the precursors in terms of reproducibility, synthesis with the selected conditions (Zn:Sn molar ratio of 1:1 for ZnAc and 2:1 for $ZnCl_2$, H_2O:EDA volume ratio of 7.5:7.5 and 0.240 M of NaOH) was repeated at least three times. The results showed a better reproducibility for $ZnCl_2$ than for the ZnAc precursor as discussed next. Figure S16a shows that for three syntheses in the same conditions using $ZnCl_2$ the results are very similar, showing only some differences in the presence of some residual ZnO NWs (confirmed by XRD spectra, in Figure S17b) and some variation in the average size of the $ZnSnO_3$ NWs (Figure 8b). On the other hand, for the synthesis with ZnAc, three runs already show a quite significant variation on the XRD spectra (Figure S17a), even if all show the predominance of the $ZnSnO_3$ phase (see also SEM images in Figure S16b). Furthermore, the size of the obtained NWs differs substantially for the multiple runs with ZnAc (Figure 8a). As discussed previously, ZnAc has a poor solubility in EDA when compared with $ZnCl_2$ and $SnCl_4 \cdot 5H_2O$. This can be one of the factors for the poor reproducibility when using ZnAc as zinc precursor. Moreover, when using $ZnCl_2$, since tin precursor is also a

DOI: 10.1021/acsanm.8b00743
ACS Appl. Nano Mater. XXXX, XXX, XXX−XXX

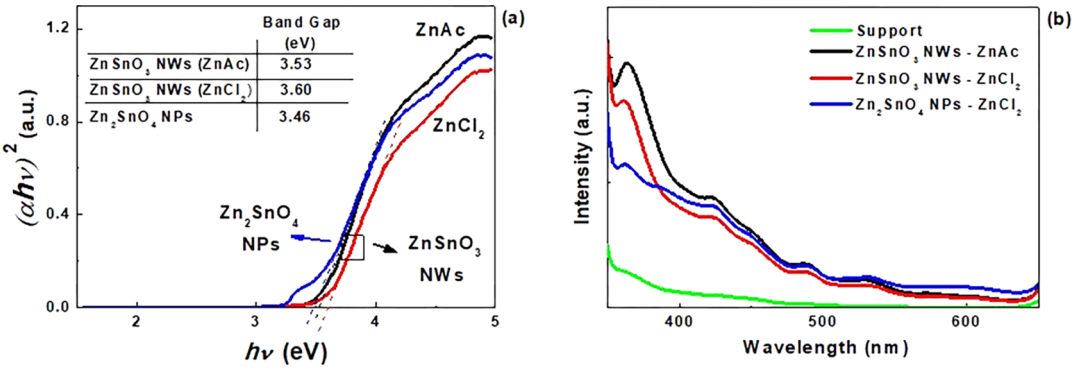

Figure 9. Tauc's plots (a) and photoluminescence spectra (b) for $ZnSnO_3$ NWs using two different zinc precursors ZnAc and $ZnCl_2$ and for Zn_2SnO_4 octahedrons, obtained using $ZnCl_2$ precursor with only H_2O as solvent.

chloride, the reaction will be less complex: not only is the number of chemical species lower, but also as Cl^- reacts with Na^+, the number of possible reactions reduces. Also, in the case of ZnAc, the presence of the ionic species H^+, O^{2-}, and C^+ can lead to an imbalance in the reaction precluding the formation of zinc tin oxide nanostructures.

$ZnSnO_3$ Nanowires: Optical and Electrical Characterization. *Optical Characterization.* To study the optical properties of the produced $ZnSnO_3$ NWs, the absorption under UV and visible radiation was measured. Figure 9a shows the well-known Tauc relation that follows the equation

$$(\alpha h\nu)^x = A(h\nu - E_g)$$

where α is the absorption coefficient, h is the Planck constant, ν is the frequency, A is an energy-independent parameter, E_g is the optical band gap, and x is a coefficient related to the electronic transition (x = 2 for allowed direct transition[63]). The E_g values, inferred by applying the equation to the linear region of the plots, are 3.53 and 3.60 eV for the ZnAc and $ZnCl_2$ precursors, respectively. For comparison, optical properties of pure Zn_2SnO_4 NPs, produced when using only H_2O as a solvent (section Influence of the Surfactant Concentration), were also evaluated (Figure 9b). A band gap of 3.46 eV was achieved, lower than for the $ZnSnO_3$ phase, confirming the trends verified by other authors.[12,17,18] These results also confirm the trends typically observed in multicomponent oxides, where the E_g of the resulting structure tends to be closer to the E_g of the predominant binary compound (ZnO or SnO_2).[64]

Still, the E_g values obtained in this work (for both $ZnSnO_3$ and Zn_2SnO_4) are slightly lower than the ones reported in literature (~0.15−0.30 eV). This difference can be explained by a higher defect density in these nanostructures, resulting in absorption close to band edges.[65] This is a consequence of the low temperature of the reported solution-based process (200 °C) as compared to the >600 °C typically used for physical processes. These band gap values suggest a potential applicability of these nanostructures for photocatalysis and photosensors.[66,67]

Photoluminescence (PL) was also evaluated for these samples (Figure 9b). A more evident peak at around 366 nm is observed, which can be attributed to ZnO-based nanostructures.[68] By observing the PL spectra, it is clear that this peak is more evident in the samples where ZnO-based structures were identified (see for instance Table S2), corroborating our previous analysis. Small peaks at 427 and 488 nm can also be identified. The presence of these UV peaks is associated with oxygen vacancies, which are major defects in this type of material,[69,70] emissions in this region being common for ZTO nanostructures.[71] Other authors also attribute a 428 nm PL peak to SnO contaminations or nanocrystals formed during ZTO synthesis,[67] which is also a plausible justification for our samples.

Electrical Characterization. Electrical measurements on single NWs, although highly desirable for determining its electrical properties, presents itself as a real challenge. In the literature the reported characterizations are related to NWs with lengths of >10 μm. In this work we present electrical characterization of a single NW with length below 1 μm. The data discussed below are for a single NW with length and diameter of 769 and 63 nm, respectively, produced using $ZnCl_2$ precursor, with a Zn:Sn molar ratio of 2:1, H_2O:EDA volume ratio of 7.5:7.5 mL, and 0.240 M of NaOH. This condition was selected based on the fact that it is the one enabling higher reproducibility and a larger fraction of dispersed $ZnSnO_3$ NW as the synthesis product. The electrical measurement was performed inside SEM using nanomanipulators after in situ deposition of Pt electrodes (Figure 10). The

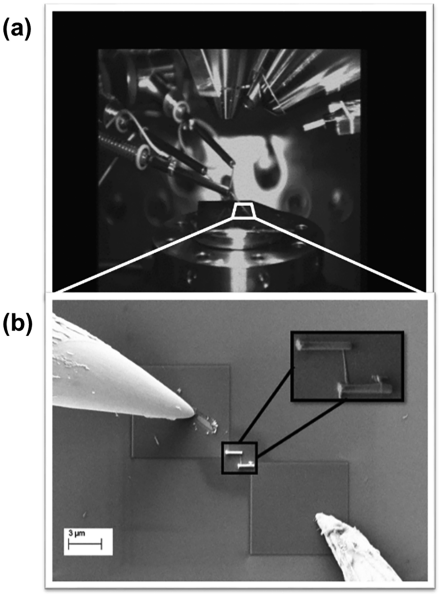

Figure 10. Images of (a) SEM nanomanipulators and (b) the W tips of the nanomanipulators contacting the Pt electrodes during electrical characterization of a single ZTO NW.

DOI: 10.1021/acsanm.8b00743
ACS Appl. Nano Mater. XXXX, XXX, XXX−XXX

obtained data (Figure 11) show linear $I-V$ characteristics, following an ohmic behavior. The background current between

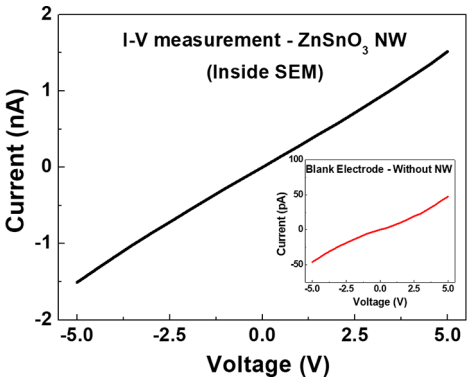

Figure 11. $I-V$ curve for a single $ZnSnO_3$ NW contacted by two Pt electrodes, measured inside SEM using nanomanipulators. The inset shows an $I-V$ curve used for background current extraction, taken from a similar sized Pt electrode structure but without any NW connecting.

two electrodes deposited in the same configuration and distance (but without a NW connecting them) was also measured, as shown in the inset of Figure 11. This background current, resulting from a residual deposition of the electrodes material over the sample, was taken into account on the calculation of the NW resistivity. The significantly lower background current level compared to the actual measurement performed in the NW reinforces the validity of the nanostructure measurement. Considering Ohm's law and the physical dimensions of the NW, a resistivity of 1.42 kΩ·cm was obtained, which is significantly higher than the one reported by Xue et al. (~73 Ω·cm)[72] for $ZnSnO_3$ NWs and by Karthik et al. (6 Ω·cm in vacuum) for Zn_2SnO_4 NWs.[67]

As explained for the optical properties analysis, the higher defect density associated with the low-temperature solution-based process is the most plausible explanation for the higher electrical resistivity reported here (Xue et al.[72] synthesized NWs by thermal evaporation at 990 °C and Karthik et al.[67] synthesized by vapor phase methods at 900 °C).

We consider that concluding whether the resistivity obtained here is too high for our targeted electronic applications would require device fabrication, e.g., field-effect transistors, where many other challenges need to be addressed, such as contact properties or electrostatic coupling between dielectric and semiconductor NW. Even if the synthesized ZTO NWs are too resistive for a certain application, there is still room for improvement, for instance, by passivation of surface-related defects by postannealing in different environments and/or by coating with encapsulation films.[73,74]

CONCLUSIONS

$ZnSnO_3$ NWs produced by a solution process without the use of a seed layer and with temperatures of only 200 °C were reported for the first time. To accomplish this, the work presented a detailed study on the influence of the different chemical parameters on the hydrothermal synthesis of ZTO nanostructures. More specifically the role of Zn:Sn ratio, surfactant concentration (EDA), and mineralization agent (NaOH) concentration for two zinc precursors (ZnAc and $ZnCl_2$) was studied. By adjustment of these parameters, the potential to achieve ZTO structures with different phases and morphologies was shown. It was found that an intricate interdependence of the different chemical parameters would enable multiple synthesis conditions to result in the final goal of obtaining ZTO NWs. Still, it was concluded that $ZnCl_2$ allowed for a more stable (with less mixture of phases/structures) and more reproducible reaction than ZnAc, with longer $ZnSnO_3$ NWs being obtained. Hence, the best condition proved to be using $ZnCl_2$ as zinc precursor, with a Zn:Sn molar ration of 2:1, H_2O:EDA volume ratio of 7.5:7.5 mL:mL, and a NaOH concentration of 0.240 M. These $ZnSnO_3$ NWs presented lengths and diameters of around 600 and 65 nm, respectively. Electrical characterization of a single NW with a length of <1 μm was successfully done inside SEM, using Pt electrodes deposited by localized e-beam assisted gas decomposition. Optical and electrical properties were comparable with those reported for ZTO NWs produced by physical processes, which employ considerably higher fabrication temperatures. As such, low-temperature hydrothermal methods proved to be a low-cost, reproducible, and highly flexible route to obtain multicomponent oxide nanostructures, particularly ZTO NWs. Moreover optical and electrical properties showed a great potential for applications such as photocatalysis, nanogenerators, nanotransistors, and gas senors/photosensors.

EXPERIMENTAL SECTION

Synthesis of Nanostructures. ZTO nanostructures were synthesized via hydrothermal method, using a modified version of the synthesis reported by Li et al.,[12] without the use of a seed layer (in ref 12 a stainless steel mesh seed-layer is used). Figure S18a shows the schematic of the synthesis where the precursor concentrations used were 0.020 M $SnCl_4{\cdot}5H_2O$ and 0.040 M $Zn(CH_3COO)_2{\cdot}2H_2O$. The precursors were separately dissolved in 7.5 mL of Millipore water and were then mixed together. Afterward, 7.5 mL of the surfactant ethylenediamine (EDA) were added, and the mixture was left stirring for 30 min. Finally 0.240 M NaOH was added. The precursors were smashed in a mortar before being added to water to help dissolution. The reagents used were all commercially available: zinc acetate dihydrate 99.0% ($Zn(CH_3COO)_2{\cdot}2H_2O$), sodium hydroxide ≥98% (NaOH), and ethylenediamine 99% (EDA) from Sigma-Aldrich, tin(IV) chloride 5-hydrate ($SnCl_4{\cdot}5H_2O$) extra pure from Riedel-de Haën and zinc chloride 98% ($ZnCl_2$) from Merck.

To study the influence of the zinc precursor, zinc acetate was replaced by zinc chloride, maintaining the same concentration of zinc in the solution. Different Zn:Sn ratios (molar concentration) were studied, namely, 2:1, 1:1, and 1:2. The ratio between H_2O and EDA was varied (H_2O:EDA, 15:0, 9:6, 8:7, 7.5:7.5, 7:8, 6:9, 0:15), as well as the concentration of NaOH (0.100 M, 0.175 M, 0.240, and 0.350 M). When the solution was ready, it was transferred into a 45 mL Teflon-lined stainless-steel autoclave, filling 80% of the total autoclave volume. The mixture was kept in an electric oven (Thermo Scientific) at 200 °C for 24 h, with a heating ramp of 200 °C/h. The autoclave was cooled to ambient temperature naturally. The resultant precipitate, comprising the nanostructures, was centrifuged at 4000 rpm and washed several times with deionized water and isopropyl alcohol, alternately. The nanostructures were finally dried at 60 °C, in vacuum, for 2 h, as schematized in Figure S18b.

Characterization of Nanostructures. Structural characterization by X-ray diffraction (XRD) was performed using a PANalytical's X'Pert PRO MRD diffractometer with Cu Ka radiation. The XRD data were acquired in the 10−90° 2θ range with a step size of 0.033°, using the nanostructures in the form of powder. Fourier transform infrared (FTIR) spectroscopy data were recorded using an attenuated total reflectance (ATR) sampling accessory (Smart iTR) equipped with a single bounce diamond crystal on a Thermo Nicolet 6700 spectrometer. The spectra were acquired with a 45° incident angle in the range of 4000−525 cm^{-1} and with a 4 cm^{-1} resolution. Raman

DOI: 10.1021/acsanm.8b00743
ACS Appl. Nano Mater. XXXX, XXX, XXX−XXX

spectroscopy measurements were carried out in a Renishaw inVia Reflex micro-Raman spectrometer equipped with an air-cooled CCD detector and a HeNe laser operating at 50 mW of 532 nm laser excitation. The spectral resolution of the spectroscopic system is 0.3 cm^{-1}. The laser beam was focused with a 50× Leica objective lens (N Plan EPI) with a numerical aperture of 0.75. An integration time of 2 scans (10 s each) was used for all measurements to reduce the random background noise induced by the detector, without significantly increasing the acquisition time. The intensity of the incident laser was 50 μW. All spectra were obtained in triplicate for each sample at room temperature in the 100−1600 nm range. After measurements a baseline subtraction was performed in order to identify the different vibrational bands. The band gap of the ZTO nanostructures was estimated from reflectance spectra recorded in the 200−800 nm range with a PerkinElmer lambda 950 UV/vis/NIR spectrophotometer using the Tauc plot method. The photoluminescence (PL) measurements were performed at room temperature, using a PerkinElmer LS.55 instrument with a xenon lamp as excitation source with an excitation wavelength of 325 nm. The morphology and element analysis of the samples were performed using scanning electron microscopy (SEM) and energy dispersive X-ray spectroscopy (EDS) inside a Carl Zeiss AURIGA CrossBeam workstation. The electrical characterization of single-NWs using a two-point probe structure was also performed inside the Auriga system. First, the NWs were dispersed in isopropyl alcohol, yielding a low concentration solution, sonicated during 5 min, and were finally drop-casted on a Si/SiO_2 substrate. After drying, isolated NWs were contacted by Pt electrodes, deposited using localized e-beam assisted decomposition of a $C_5H_4CH_3Pt(CH_3)_3$ precursor introduced close to the sample surface using a gas injector system. Kleindiek nanomanipulators with W tips were then used to access the current−voltage characteristics, together with a semiconductor parameter analyzer (Agilent 4155 C).

■ ASSOCIATED CONTENT

Supporting Information

The Supporting Information is available free of charge on the ACS Publications website at DOI: 10.1021/acsanm.8b00743.

Figures showing (1) crystal structures, (2) X-ray diffraction pattern, (3) FTIR spectra before and after synthesis, (5−12) SEM/EDS analysis, (4, 13) Raman spectroscopy related to the studies of Zn:Sn molar ratio and of the H_2O:EDA volume ratio, respectively, and (14) FTIR spectra regarding the study of the surfactant concentration; Tables S1, S2, and S3 summarizing the obtainable nanostructures and its dimensions for each of the chemical parameters in study (PDF)

■ AUTHOR INFORMATION

Corresponding Author

*E-mail: pmcb@fct.unl.pt.

ORCID

Ana Rovisco: 0000-0001-6240-3743

Rita Branquinho: 0000-0001-9771-8366

Elvira Fortunato: 0000-0002-4202-7047

Author Contributions

A.R. designed the experiments, fabricated the nanostructures, performed the data analysis, and wrote the manuscript. J.M. supported the electrical characterization and its analysis and also provided support to manuscript preparation. M.J.O. performed the Raman characterization. D.G. provided the SEM/EDS characterization. P.B. and R.B. supervised the work and revised the concept, structure, and content of the different versions of the manuscript until its final form. R.M. and E.F. provided the fabrication and characterization facilities and reviewed the final versions of the manuscript.

Notes

The authors declare no competing financial interest.

■ ACKNOWLEDGMENTS

This work is funded by FEDER funds through the COMPETE 2020 Programme and national funds through FCT—Portuguese Foundation for Science and Technology under Project POCI-01-0145-FEDER-007688, Reference UID/CTM/50025, and the Doctoral Grant Research Number SFRH/BD/131836/2017. This work also received funding from the European Community's H2020 program under Grant Agreement 716510 (ERC-2016-STG TREND), Grant 685758 (1D-Neon), and Grant 692373 (BET-EU).

■ REFERENCES

(1) Roselli, L.; Borges Carvalho, N.; Alimenti, F.; Mezzanotte, P.; Orecchini, G.; Virili, M.; Mariotti, C.; Goncalves, R.; Pinho, P. Smart Surfaces: Large Area Electronics Systems for Internet of Things Enabled by Energy Harvesting. Proc. *Proc. IEEE* **2014**, *102*, 1723−1746.

(2) Schmidt-Mende, L.; MacManus-Driscoll, J. L. ZnO - Nanostructures, Defects, and Devices. Mater. *Mater. Today* **2007**, *10*, 40−48.

(3) Kołodziejczak-Radzimska, A.; Jesionowski, T. Zinc Oxide—From Synthesis to Application: A Review. *Materials* **2014**, *7*, 2833−2881.

(4) Zhao, Y.; Lai, X.; Deng, P.; Nie, Y.; Zhang, Y.; Xing, L.; Xue, X. Pt/ZnO Nanoarray Nanogenerator as Self-Powered Active Gas Sensor with Linear Ethanol Sensing at Room Temperature. *Nanotechnology* **2014**, *25*, 115502.

(5) Zhao, Y.; Deng, P.; Nie, Y.; Wang, P.; Zhang, Y.; Xing, L.; Xue, X. Biomolecule-Adsorption-Dependent Piezoelectric Output of ZnO Nanowire Nanogenerator and Its Application as Self-Powered Active Biosensor. *Biosens. Bioelectron.* **2014**, *57*, 269−275.

(6) Pang, C.; Yan, B.; Liao, L.; Liu, B.; Zheng, Z.; Wu, T.; Sun, H.; Yu, T. Synthesis, Characterization and Opto-Electrical Properties of Ternary Zn_2SnO_4 Nanowires. *Nanotechnology* **2010**, *21*, 465706.

(7) Mancini, L.; Sala, S.; Recchioni, M.; Benini, L.; Goralczyk, M.; Pennington, D. Potential of Life Cycle Assessment for Supporting the Management of Critical Raw Materials. *Int. J. Life Cycle Assess.* **2015**, *20*, 100−116.

(8) Guo, R.; Guo, Y.; Duan, H.; Li, H.; Liu, H. Synthesis of Orthorhombic Perovskite-Type $ZnSnO_3$ Single-Crystal Nanoplates and Their Application in Energy Harvesting. *ACS Appl. Mater. Interfaces* **2017**, *9*, 8271−8279.

(9) Wu, J. M.; Chen, C.-Y.; Zhang, Y.; Chen, K.-H.; Yang, Y.; Hu, Y.; He, J.-H.; Wang, Z. L. Ultrahigh Sensitive Piezotronic Strain Sensors Based on a $ZnSnO_3$ Nanowire/Microwire. *ACS Nano* **2012**, *6*, 4369−4374.

(10) Baruah, S.; Dutta, J. Zinc Stannate Nanostructures: Hydrothermal Synthesis. *Sci. Technol. Adv. Mater.* **2011**, *12*, 013004.

(11) Sun, S.; Liang, S. Morphological Zinc Stannate: Synthesis, Fundamental Properties and Applications. *J. Mater. Chem. A* **2017**, *5*, 20534−20560.

(12) Li, Z.; Zhou, Y.; Bao, C.; Xue, G.; Zhang, J.; Liu, J.; Yu, T.; Zou, Z. Vertically Building Zn_2SnO_4 Nanowire Arrays on Stainless Steel Mesh toward Fabrication of Large-Area, Flexible Dye-Sensitized Solar Cells. *Nanoscale* **2012**, *4*, 3490−3494.

(13) Lo, M.-K.; Lee, S.-Y.; Chang, K.-S. Study of $ZnSnO_3$-Nanowire Piezophotocatalyst Using Two-Step Hydrothermal Synthesis. *J. Phys. Chem. C* **2015**, *119*, 5218−5224.

(14) Inaguma, Y.; Yoshida, M.; Katsumata, T. A Polar Oxide $ZnSnO_3$ with a $LiNbO_3$-Type Structure. *J. Am. Chem. Soc.* **2008**, *130*, 6704−6705.

DOI: 10.1021/acsanm.8b00743
ACS Appl. Nano Mater. XXXX, XXX, XXX−XXX

(15) Dal Corso, A.; Posternak, M.; Resta, R.; Baldereschi, A. Ab Initio Study of Piezoelectricity and Spontaneous Polarization in ZnO. *Phys. Rev. B: Condens. Matter Mater. Phys.* **1994**, *50*, 10715−10721.
(16) Mao, Y.; Park, T.-J.; Wong, S. S. Synthesis of Classes of Ternary Metal Oxide Nanostructures. *Chem. Commun.* **2005**, 5721.
(17) Miyauchi, M.; Liu, Z.; Zhao, Z.-G.; Anandan, S.; Hara, K. Single Crystalline Zinc Stannate Nanoparticles for Efficient Photo-Electrochemical Devices. *Chem. Commun.* **2010**, *46*, 1529−1531.
(18) Lei, M.; Sheng, Y.; Wan, L.; Bi, K.; Huang, K.; Jia, R.; Liu, J.; Wang, Y. A Novel Self-Catalytic Route to Zinc Stannate Nanowires and Cathodoluminescence and Electrical Transport Properties of a Single Nanowire. *J. Alloys Compd.* **2016**, *657*, 394−399.
(19) Lim, T.; Kim, H.; Meyyappan, M.; Ju, S. Photostable Zn_2SnO_4 Nanowire Transistors for Transparent Displays. *ACS Nano* **2012**, *6*, 4912−4920.
(20) Annamalai, A.; Carvalho, D.; Wilson, K. C.; Lee, M.-J. Properties of Hydrothermally Synthesized Zn_2SnO_4 Nanoparticles Using Na_2CO_3 as a Novel Mineralizer. *Mater. Charact.* **2010**, *61*, 873−881.
(21) Shi, J.-B.; Wu, P.-F.; Lin, H.-S.; Lin, Y.-T.; Lee, H.-W.; Kao, C.-T.; Liao, W.-H.; Young, S.-L. Synthesis and Characterization of Single-Crystalline Zinc Tin Oxide Nanowires. *Nanoscale Res. Lett.* **2014**, *9*, 210.
(22) Lehnen, T.; Zopes, D.; Mathur, S. Phase-Selective Microwave Synthesis and Inkjet Printing Applications of Zn_2SnO_4 (ZTO) Quantum Dots. *J. Mater. Chem.* **2012**, *22*, 17732.
(23) Ji, X.; Huang, X.; Liu, J.; Jiang, J.; Li, X.; Ding, R.; Hu, Y.; Wu, F.; Li, Q. Hydrothermal Synthesis of Novel Zn_2SnO_4 Octahedron Microstructures Assembled with Hexagon Nanoplates. *J. Alloys Compd.* **2010**, *503*, L21−L25.
(24) Choi, K. H.; Siddiqui, G. U.; Yang, B.; Mustafa, M. Synthesis of $ZnSnO_3$ Nanocubes and Thin Film Fabrication of ($ZnSnO_3$/PMMA) Composite through Electrospray Deposition. *J. Mater. Sci.: Mater. Electron.* **2015**, *26*, 5690−5696.
(25) Zhou, T.; Zhang, T.; Zhang, R.; Lou, Z.; Deng, J.; Wang, L. Hollow $ZnSnO_3$ Cubes with Controllable Shells Enabling Highly Efficient Chemical Sensing Detection of Formaldehyde Vapors. *ACS Appl. Mater. Interfaces* **2017**, *9*, 14525−14533.
(26) Chen, Z.; Cao, M.; Hu, C. Novel Zn_2SnO_4 Hierarchical Nanostructures and Their Gas Sensing Properties toward Ethanol. *J. Phys. Chem. C* **2011**, *115*, 5522−5529.
(27) Najam Khan, M.; Al-Hinai, M.; Al-Hinai, A.; Dutta, J. Visible Light Photocatalysis of Mixed Phase Zinc Stannate/Zinc Oxide Nanostructures Precipitated at Room Temperature in Aqueous Media. *Ceram. Int.* **2014**, *40*, 8743−8752.
(28) Xue, X. Y.; Chen, Y. J.; Wang, Y. G.; Wang, T. H. Synthesis and Ethanol Sensing Properties of $ZnSnO_3$ Nanowires. *Appl. Phys. Lett.* **2005**, *86*, 233101.
(29) Wang, L.; Zhou, T.; Zhang, R.; Lou, Z.; Deng, J.; Zhang, T. Comparison of Toluene Sensing Performances of Zinc Stannate with Different Morphology-Based Gas Sensors. *Sens. Actuators, B* **2016**, *227*, 448−455.
(30) Zhou, T.; Zhang, T.; Zhang, R.; Deng, J.; Lou, Z.; Lu, G.; Wang, L. Highly Sensitive Sensing Platform Based on $ZnSnO_3$ Hollow Cubes for Detection of Ethanol. *Appl. Surf. Sci.* **2017**, *400*, 262−268.
(31) Wu, J. M.; Xu, C.; Zhang, Y.; Wang, Z. L. Lead-Free Nanogenerator Made from Single $ZnSnO_3$ Microbelt. *ACS Nano* **2012**, *6*, 4335−4340.
(32) Wu, J. M.; Xu, C.; Zhang, Y.; Yang, Y.; Zhou, Y.; Wang, Z. L. Flexible and Transparent Nanogenerators Based on a Composite of Lead-Free $ZnSnO_3$ Triangular-Belts. *Adv. Mater.* **2012**, *24*, 6094−6099.
(33) Fu, Y.; Nie, Y.; Zhao, Y.; Wang, P.; Xing, L.; Zhang, Y.; Xue, X. Detecting Liquefied Petroleum Gas (LPG) at Room Temperature Using $ZnSnO_3$ZnO Nanowire Piezo-Nanogenerator as Self-Powered Gas Sensor. *ACS Appl. Mater. Interfaces* **2015**, *7*, 10482−10490.
(34) Cheng, B.; Ouyang, Z.; Chen, C.; Xiao, Y.; Lei, S. Individual Zn_2SnO_4-Sheathed ZnO Heterostructure Nanowires for Efficient Resistive Switching Memory Controlled by Interface States. *Sci. Rep.* **2013**, *3*, 3249.
(35) Siddiqui, G. U.; Rehman, M. M.; Choi, K. H. Resistive Switching Phenomena Induced by the Heterostructure Composite of $ZnSnO_3$ Nanocubes Interspersed ZnO Nanowires. *J. Mater. Chem. C* **2017**, *5*, 5528−5537.
(36) Mali, S. S.; Su Shim, C.; Kook Hong, C. Highly Porous Zinc Stannate (Zn_2SnO_4) Nanofibers Scaffold Photoelectrodes for Efficient Methyl Ammonium Halide Perovskite Solar Cells. *Sci. Rep.* **2015**, *5*, 11424.
(37) Wang, Y.; Gao, P.; Bao, D.; Wang, L.; Chen, Y.; Zhou, X.; Yang, P.; Sun, S.; Zhang, M. One Pot, Two Phases: Individual Orthorhombic and Face-Centered Cubic $ZnSnO_3$ Obtained Synchronously in One Solution. *Inorg. Chem.* **2014**, *53* (23), 12289−12296.
(38) Fang, C.; Geng, B.; Liu, J.; Zhan, F. D-Fructose Molecule Template Route to Ultra-Thin $ZnSnO_3$ Nanowire Architectures and Their Application as Efficient Photocatalyst. *Chem. Commun.* **2009**, 2350.
(39) Jie, J.; Wang, G.; Han, X.; Fang, J.; Yu, Q.; Liao, Y.; Xu, B.; Wang, Q.; Hou, J. G. Growth of Ternary Oxide Nanowires by Gold-Catalyzed Vapor-Phase Evaporation. *J. Phys. Chem. B* **2004**, *108*, 8249−8253.
(40) Men, H.; Gao, P.; Zhou, B.; Chen, Y.; Zhu, C.; Xiao, G.; Wang, L.; Zhang, M. Fast Synthesis of Ultra-Thin $ZnSnO_3$ Nanorods with High Ethanol Sensing Properties. *Chem. Commun.* **2010**, *46*, 7581.
(41) Guerfi, Y.; Larrieu, G. Vertical Silicon Nanowire Field Effect Transistors with Nanoscale Gate-All-Around. *Nanoscale Res. Lett.* **2016**, *11*, 210.
(42) Larrieu, G.; Guerfi, Y.; Han, X. L.; Clément, N. Solid-State Electronics Sub-15 Nm Gate-All-around Field Effect Transistors on Vertical Silicon Nanowires. *Solid-State Electron.* **2017**, *130*, 9−14.
(43) Zeng, J.; Xin, M.; Li, K.; Wang, H.; Yan, H.; Zhang, W. Transformation Process and Photocatalytic Activities of Hydrothermally Synthesized Zn_2SnO_4 Nanocrystals. *J. Phys. Chem. C* **2008**, *112*, 4159−4167.
(44) Su, B.; Wu, Y.; Jiang, L. The Art of Aligning One-Dimensional (1D) Nanostructures. *Chem. Soc. Rev.* **2012**, *41*, 7832.
(45) Tharsika, T.; Haseeb, A. S. M. a.; Akbar, S. a.; Sabri, M. F. M.; Wong, Y. H. Gas Sensing Properties of Zinc Stannate (Zn_2SnO_4) Nanowires Prepared by Carbon Assisted Thermal Evaporation Process. *J. Alloys Compd.* **2015**, *618*, 455−462.
(46) Ju, S.; Facchetti, A.; Xuan, Y.; Liu, J.; Ishikawa, F.; Ye, P.; Zhou, C.; Marks, T. J.; Janes, D. B. Fabrication of Fully Transparent Nanowire Transistors for Transparent and Flexible Electronics. *Nat. Nanotechnol.* **2007**, *2*, 378−384.
(47) Kumari, V.; Patra, A. K.; Bhaumik, A. Self-Assembled Ultra-Small Zinc Stannate Nanocrystals with Mesoscopic Voids via a Salicylate Templating Pathway and Their Photocatalytic Properties. *RSC Adv.* **2014**, *4*, 13626−13634.
(48) Chen, Y.; Yu, L.; Li, Q.; Wu, Y.; Li, Q.; Wang, T. An Evolution from 3D Face-Centered-Cubic $ZnSnO_3$ Nanocubes to 2D Orthorhombic $ZnSnO_3$ Nanosheets with Excellent Gas Sensing Performance. *Nanotechnology* **2012**, *23*, 415501.
(49) Bora, T.; Al-Hinai, M. H.; Al-Hinai, A. T.; Dutta, J. Phase Transformation of Metastable $ZnSnO_3$ Upon Thermal Decomposition by In-Situ Temperature-Dependent Raman Spectroscopy. *J. Am. Ceram. Soc.* **2015**, *98*, 4044−4049.
(50) Song, P.; Wang, Q.; Yang, Z. Biomorphic Synthesis of $ZnSnO_3$ Hollow Fibers for Gas Sensing Application. *Sens. Actuators, B* **2011**, *156*, 983−989.
(51) Wang, Y.; Gao, P.; Bao, D.; Wang, L.; Chen, Y.; Zhou, X.; Yang, P.; Sun, S.; Zhang, M. One Pot, Two Phases: Individual Orthorhombic and Face-Centered Cubic $ZnSnO_3$ Obtained Synchronously in One Solution. *Inorg. Chem.* **2014**, *53*, 12289−12296.
(52) Placke, A.; Kumar, A.; Priya, S. Synthesis and Behavior of Cetyltrimethyl Ammonium Bromide Stabilized $Zn_{1+x}SnO_{3+x}$ ($0 \leq x \leq 1$) Nano-Crystallites. *PLoS One* **2016**, *11*, e0156246.

DOI: 10.1021/acsanm.8b00743
ACS Appl. Nano Mater. XXXX, XXX, XXX−XXX

(53) Diéguez, A.; Romano-Rodríguez, A.; Vilà, A.; Morante, J. R. The Complete Raman Spectrum of Nanometric SnO2particles. *J. Appl. Phys.* **2001**, *90*, 1550−1557.
(54) Kovacheva, D. Preparation of Crystalline $ZnSnO_3$ from Li_2SnO_3 by Low-Temperature Ion Exchange. *Solid State Ionics* **1998**, *109*, 327−332.
(55) Mao, W.; Li, Z.; Bao, K.; Zhang, K.; Wang, W.; Li, B. Nanowire-Based Zinc-Doped Tin Oxide Microtubes for Enhanced Solar Energy Utilization Efficiency. *Ceram. Int.* **2017**, *43*, 6822−6830.
(56) Pimentel, A.; Rodrigues, J.; Duarte, P.; Nunes, D.; Costa, F. M.; Monteiro, T.; Martins, R.; Fortunato, E. Effect of Solvents on ZnO Nanostructures Synthesized by Solvothermal Method Assisted by Microwave Radiation: A Photocatalytic Study. *J. Mater. Sci.* **2015**, *50*, 5777−5787.
(57) Tian, Z. R.; Voigt, J. A.; Liu, J.; Mckenzie, B.; Mcdermott, M. J.; Rodriguez, M. A.; Konishi, H.; Xu, H. Complex and Oriented ZnO Nanostructures. *Nat. Mater.* **2003**, *2*, 821−826.
(58) Ivetić, T. B.; Finčur, N. L.; Đačanin, L. R.; Abramović, B. F.; Lukić-Petrović, S. R. Ternary and Coupled Binary Zinc Tin Oxide Nanopowders: Synthesis, Characterization, and Potential Application in Photocatalytic Processes. *Mater. Res. Bull.* **2015**, *62*, 114−121.
(59) Zhao, Q.; Ju, D.; Song, X.; Deng, X.; Ding, M.; Xu, X.; Zeng, H. Polyhedral Zn_2SnO_4: Synthesis, Enhanced Gas Sensing and Photocatalytic Performance. *Sens. Actuators, B* **2016**, *229*, 627−634.
(60) Li, J.; Chen, Z.; Wang, R. J.; Proserpio, D. M. Low Temperature Route towards New Materials: Solvothermal Synthesis of Metal Chalcogenides in Ethylenediamine. *Coord. Chem. Rev.* **1999**, *190−192*, 707−735.
(61) Liu, Q.; Zhou, Y.; Kou, J.; Chen, X.; Tian, Z.; Gao, J.; Yan, S.; Zou, Z. High-Yield Synthesis of Ultralong and Ultrathin Zn_2GeO_4 Nanoribbons toward Improved Photocatalytic Reduction of CO2 into Renewable Hydrocarbon Fuel. *J. Am. Chem. Soc.* **2010**, *132*, 14385−14387.
(62) Xu, S.; Wang, Z. L. One-Dimensional ZnO Nanostructures: Solution Growth and Functional Properties. *Nano Res.* **2011**, *4*, 1013−1098.
(63) Pimentel, A.; Ferreira, S.; Nunes, D.; Calmeiro, T.; Martins, R.; Fortunato, E. Microwave Synthesized ZnO Nanorod Arrays for UV Sensors: A Seed Layer Annealing Temperature Study. *Materials* **2016**, *9*, 299.
(64) Barquinha, P. *Transparent Oxide Electronics: From Materials to Devices*; Wiley InterScience, 2012.
(65) Barquinha, P.; Pereira, L.; Gonçalves, G.; Martins, R.; Kuščer, D.; Kosec, M.; Fortunato, E. Performance and Stability of Low Temperature Transparent Thin-Film Transistors Using Amorphous Multicomponent Dielectrics. *J. Electrochem. Soc.* **2009**, *156*, H824.
(66) An, Q.; Meng, X.; Xiong, K.; Qiu, Y. Self-Powered ZnS Nanotubes/Ag Nanowires MSM UV Photodetector with High On/Off Ratio and Fast Response Speed. *Sci. Rep.* **2017**, *7*, 1−12.
(67) Karthik, K. R. G.; Andreasson, B. P.; Sun, C.; Pramana, S. S.; Varghese, B.; Sow, C. H.; Mathews, N.; Wong, L. H.; Mhaisalkar, S. G. Physical and Electrical Properties of Single Zn_2SnO_4 Nanowires. *Electrochem. Solid-State Lett.* **2011**, *14*, K5.
(68) Zhao, J. H.; Liu, C. J.; Lv, Z. H. Photoluminescence of ZnO Nanoparticles and Nanorods. *Optik (Munich, Ger.)* **2016**, *127*, 1421−1423.
(69) Shewale, P. S.; Ung Sim, K.; Kim, Y.-b.; Kim, J. H.; Moholkar, A. V.; Uplane, M. D. Structural and Photoluminescence Characterization of SnO2: F Thin Films Deposited by Advanced Spray Pyrolysis Technique at Low Substrate Temperature. *J. Lumin.* **2013**, *139*, 113−118.
(70) Mageshwari, K.; Kim, T. G.; Park, J. Effect of Alkaline Concentration on the Structural and Luminescence Properties of $ZnSnO_3$ Nanoparticles Obtained by Facile Reflux Method. *J. Mater. Sci.: Mater. Electron.* **2016**, *27*, 4093−4097.
(71) Wang, J. X.; Xie, S. S.; Gao, Y.; Yan, X. Q.; Liu, D. F.; Yuan, H. J.; Zhou, Z. P.; Song, L.; Liu, L. F.; Zhou, W. Y.; et al. Growth and Characterization of Axially Periodic Zn_2SnO_4 (ZTO) Nanostructures. *J. Cryst. Growth* **2004**, *267*, 177−183.
(72) Xue, X. Y.; Chen, Y. J.; Li, Q. H.; Wang, C.; Wang, Y. G.; Wang, T. H. Electronic Transport Characteristics through Individual $ZnSnO_3$ Nanowires. *Appl. Phys. Lett.* **2006**, *88*, 182102.
(73) Chang, P.-C.; Lu, J. G. ZnO Nanowire Field-Effect Transistors. *IEEE Trans. Electron Devices* **2008**, *55*, 2977−2987.
(74) Park, W. Il; Kim, J. S.; Yi, G. C.; Bae, M. H.; Lee, H. J. Fabrication and Electrical Characteristics of High-Performance ZnO Nanorod Field-Effect Transistors. *Appl. Phys. Lett.* **2004**, *85*, 5052−5054.

DOI: 10.1021/acsanm.8b00743
ACS Appl. Nano Mater. XXXX, XXX, XXX−XXX